field. For an ellipsoid with a severe flattening of 2/3, J_2 reaches 0.25 and the correction to the mass is on the order of 4%.
22. Radar astrometry was published in MPEC 2001-Q33.
23. The large uncertainty is due primarily to the 60% relative uncertainty on volume (three times the relative uncertainty on the radius of the primary). The application of shape-modeling techniques (*15*) is expected to improve the size estimate and to reduce those error bars considerably.
24. G. J. Consolmagno, D. T. Britt, *Meteorit. Planet. Sci.* **33**, 1231 (1998).
25. J. Veverka *et al.*, *Icarus*, **140**, 3 (1999).
26. The height at which an orbiting secondary has a revolution period equal to the spin period of the primary is called the synchronous height. It is only a few meters above the surface of the primary in this case.
27. The tidal torque and rate of change in a are proportional to the k_2 Love number of the primary, i.e., its response coefficient to a centrifugal potential, and are inversely proportional to the tidal dissipation factor Q (*52*):

$$\dot{a} = 3\frac{k_2}{Q}\frac{M_s}{M_p}\left(\frac{R_p}{a}\right)^5 na \qquad (2)$$

where M_s and M_p are the masses of the secondary and primary, respectively, and other quantities have been defined in the text. Solving for k_2/Q after integration,

$$\frac{k_2}{Q} = \frac{2}{39}\frac{M_p}{M_s}\left(\frac{a}{R_p}\right)^5\frac{1}{nT} \qquad (3)$$

where T is the time scale for orbital evolution. This ratio is related to material properties through $k_2 = [(3/2)/(1+\tilde{\mu})]$ and $\tilde{\mu} = 19\mu/2\rho g R_p$, where g is the surface gravity, μ is the rigidity or shear modulus, and $\tilde{\mu}$ is the effective rigidity or ratio of elastic and gravitational forces.
28. B. J. Gladman *et al.*, *Science* **277**, 197 (1997).
29. P. Goldreich, S. Soter, *Icarus* **5**, 375 (1966).
30. The tidal despinning time scale is given by

$$\tau = \frac{4}{15}\frac{Q}{k_2}\frac{M_s}{M_p^2}\frac{a^6}{R_s^3}\frac{\Delta\omega}{G} \qquad (4)$$

where $\Delta\omega$ is the change in spin rate (*52*).
31. Although the specific binding energy of this system is less than 0.01 J, it can probably survive gentle orbital perturbations that act on time scales much longer than the revolution period of the satellite. For instance, drift rates due to the Yarkovsky effect are on the order of 10^{-4} AU/My (*53*).
32. S. J. Weidenschilling, P. Paolicchi, V. Zappalà, in *Asteroids II*, R. P. Binzel, T. Gehrels, M. S. Matthews, Eds. (Univ. of Arizona Press, Tucson, 1989), p. 643.
33. D. D. Durda, *Icarus* **120**, 212 (1996).
34. T. C. Van Flandern, E. F. Tedesco, R. P. Binzel, in *Asteroids I*, T. Gehrels, Ed. (Univ. of Arizona Press, Tucson, 1979), p. 443.
35. W. K. Hartmann, in *Asteroids I*, T. Gehrels, Ed. (Univ. of Arizona Press, Tucson, 1979), p. 466.
36. S. J. Weidenschilling, *Icarus* **44**, 807 (1980).
37. The breakup rate of a fluid or strengthless body occurs when the synchronous height (*26*) corresponds to the radius of the object itself. The critical rotation period expressed in hours is $P_{crit} = 3.3/\sqrt{\rho}$, or 2.5 hours for the nominal density of 2000 DP107.
38. W. F. Bottke Jr., H. J. Melosh, *Nature* **381**, 51 (1996).
39. E. Asphaug, W. Benz, *Icarus* **121**, 225 (1996).
40. D. C. Richardson, W. F. Bottke Jr., S. G. Love, *Icarus* **134**, 47 (1998).
41. S. Sridhar, S. Tremaine, *Icarus* **95**, 86 (1992).
42. The Roche limit is the semimajor axis within which a prograde and strengthless satellite is disrupted by planetary tidal forces. It is given by $R_{roche} = 2.45R_p(\rho_p/\rho_s)^{1/3}$, where ρ_p and ρ_s are the densities of the planet and satellite, respectively.
43. Because the system's total angular momentum is conserved during orbital expansion, the spin angular momentum must decrease whereas the orbital momentum increases. [In the Earth-Moon system, this process accounts for the lengthening of the day at a rate of ~1.6 ms/cy and the recession of the Moon at a rate of ~3.8 m/cy (*52*).] Conversely, if the secondary formed near the primary, the primary's spin angular momentum must have been larger at the time of formation by an amount equal to the current orbital angular momentum.
44. The primary of 2000 DP107 spins at a rate close to the maximum rate that a strengthless body of density 1.7 g cm^{-3} can sustain without disruption (*37*). The addition of the orbital angular momentum, $\sim 6.7 \times 10^{12}$ kg m^2 s^{-1}, to the primary's spin angular momentum, $\sim 1.8 \times 10^{13}$ kg m^2 s^{-1}, would result in a 2-hour spin period at the time of formation, which is below the critical period to avoid breakup (*37*).
45. Pravec and Harris (*6*) do not observe spin periods smaller than 2.2 hours in the sample of asteroids larger than 200 m. They interpret the sharp truncation in spin rates as evidence that most asteroids larger than a few hundred meters in size are gravitationally bound aggregates. Because such aggregates are more prone to tidal fission than monolithic bodies, this notion and the observed size threshold are consistent with the formation of asteroid binaries by tidal disruption.
46. W. J. Merline *et al.*, *Nature* **401**, 565 (1999).
47. W. J. Merline *et al.*, IAU Circ. No. 7503 (2000).
48. W. J. Merline *et al.*, IAU Circ. No. 7827 (2002).
49. M. E. Brown, J. L. Margot, IAU Circ. No. 7588 (2001).
50. J. L. Margot, M. E. Brown, IAU Circ. No. 7703 (2001).
51. R. Greenberg, *Astron. J.* **86**, 912 (1981).
52. S. J. Peale, *Annu. Rev. Astron. Astrophys.* **37**, 533 (1999).
53. P. Farinella, D. Vokrouhlický, W. K. Hartmann, *Icarus* **132**, 378 (1998).
54. There is a fundamental inclination ambiguity in the determination of orbits from range-Doppler data obtained with poor orientational coverage. Observations over a range of aspect angles can overcome this ambiguity. By combining the Goldstone and Arecibo data, the angular leverage for 2000 DP107 corresponds to 40° of sky motion. The detection of occultations in the radar data or of occulations or eclipses in the lightcurve data can also place strong constraints on the inclination of the orbit. In general, a combination of radar and lightcurve observations will yield the best orbital determinations.
55. To test the robustness of our solution against measurement errors, we generated 99 synthetic data sets by adding random noise to our measurements, with the standard deviation of the noise corresponding to our measurement uncertainties scaled by the square root of reduced χ^2. Each synthetic data set underwent the same minimization procedure as the actual data. We find that most solutions fall within our quoted uncertainties, with the exception of pathologic solutions in narrow valleys of the χ^2 space. The pathologic solutions have large semimajor axes and orbital inclinations with respect to the line-of-sight (*54*). They can be discarded because their geometry does not allow for occultation or eclipse events reported from lightcurve observations (*18*).
56. We thank P. Nicholson, P. Goldreich, W. Bottke, and E. Asphaug for fruitful discussions on tidal deformation and evolution, and the staffs at Goldstone and Arecibo for assistance with the observations. J.L.M. thanks S. Kulkarni for financial support. The Arecibo Observatory is part of the National Astronomy and Ionosphere Center, which is operated by Cornell University under a cooperative agreement with the National Science Foundation and with support from NASA. This work was supported in part by the Jet Propulsion Laboratory, operated by the California Institute of Technology under contract with NASA.

21 March 2002; accepted 3 April 2002
Published online 11 April 2002;
10.1126/science.1072094
Include this information when citing this paper.

Metasomatic Origin of Quartz-Pyroxene Rock, Akilia, Greenland, and Implications for Earth's Earliest Life

Christopher M. Fedo[1]* and Martin J. Whitehouse[2]

A quartz-pyroxene rock interpreted as a banded iron formation (BIF) from the island of Akilia, southwest Greenland, contains ^{13}C-depleted graphite that has been claimed as evidence for the oldest (>3850 million years ago) life on Earth. Field relationships on Akilia document multiple intense deformation events that have resulted in parallel transposition of Early Archean rocks and significant boudinage, the tails of which commonly form the banding in the quartz-pyroxene rock. Geochemical data possess distinct characteristics consistent with an ultramafic igneous, not BIF, protolith for this lithology and the adjacent schists. Later metasomatic silica and iron introduction have merely resulted in a rock that superficially resembles a BIF. An ultramafic igneous origin invalidates claims that the carbon isotopic composition of graphite inclusions represents evidence for life at the time of crystallization.

On the island of Akilia, outer Gothåbsfjord, southwest Greenland (Fig. 1, A and B), a sequence of lithologies that has been interpreted as mafic volcanic rocks intercalated with silicious sedimentary rocks chemically precipitated from seawater [banded iron formation (BIF)] contains carbon isotopic signatures that have been interpreted as perhaps the oldest known life on Earth [>3850 million years ago (Ma)] (*1*–*3*), overlapping in age with potentially planet-sterilizing asteroid impacts (*4*, *5*). Here we present new geologic, petrologic, and geochemical evidence that favors a metasomatized ultramafic

[1]Department of Earth and Environmental Sciences, George Washington University, Washington, DC 20052, USA. [2]Swedish Museum of Natural History, Laboratory for Isotope Geology, Box 50007, SE-104 05 Stockholm, Sweden.

*To whom correspondence should be addressed. E-mail: cfedo@gwu.edu

igneous origin for rocks previously considered to be BIFs, indicating that it is highly improbable that the rocks hosted life at the time of their formation.

There are two main lithologic groups on Akilia: (i) ~3650 to (?) >3850 million-year-old composite, banded, tonalitic Amîtsoq gneisses (*6*–*9*) and (ii) coarse-grained mafic/ultramafic rocks, termed the Akilia association (*10*), which are generally assumed to be older. On Akilia, mafic and ultramafic rocks host a distinct, banded quartz-pyroxene lithology that has been interpreted as a BIF (*1*–*3*, *10*). All rocks have experienced polyphase regional metamorphism, including a granulite facies event [temperature (T) > ~600°C, pressure (P) > 8 kbar] at ~3600 Ma (*11*) and an upper amphibolite facies event at ~2700 Ma (*6*), which have imposed a penetrative tectonic fabric (*12*) in such a way that all lithologies are strongly schistose (or banded) and have been transposed into parallelism.

The postulated chemical sedimentary protolith for banded quartz-pyroxene rocks on Akilia (Figs. 1C and 2) is an essential prerequisite for the interpretation of carbon isotope signatures as evidence for life (*1*), because it would establish the existence of a liquid hydrosphere in a habitable temperature range. Such a protolith has been proposed (*1*–*3*) on the basis of (i) apparent depositional conformity with mafic/ultramafic rocks, assumed to represent basaltic/komatiitic flows (*2*), that were intruded by tonalite at ~3850 Ma; (ii) pronounced layering inferred to be a primary depositional feature; and (iii) similarity to BIFs in the Isua greenstone belt.

Considerable controversy (*7*, *9*, *12*) has attended the assignment of a >3850-Ma age to the mafic/ultramafic assemblage and, by inference, the purported BIF, based on complex U-Pb zircon age spectra from claimed cross-cutting Amîtsoq gneiss sheets (*2*). Our new geologic mapping has not identified a clear igneous cross-cutting relationship with the quartz-pyroxene lithology, nor with the adjacent mafic/ultramafic rocks, which have been considered as extrusive (*2*) but could easily represent ultramafic intrusions [for example, Isua, (*13*)]. Amîtsoq gneisses commonly exhibit sheared-out intrafolial fold limbs that leave relic fold hinges in angular juxtaposition with adjacent gneissic bands, a discordance that clearly has no protolith age significance. Consequently, any presently observed discordance between relatively homogeneous mafic/ultramafic rocks and Amîtsoq gneisses is similarly likely to be a later tectonic feature (*12*) and not a primary igneous relationship (*2*). Direct dating has yielded a lower age limit of ~3.7 billion years ago for the host mafic/ultramafic rocks themselves (*8*, *9*).

The banding or layering in the quartz-pyroxene rock (Fig. 2), in which boudinage is common, is coaxial with the penetrative schistosity developed in adjacent mafic/ultramafic rocks. In these intensely deformed rocks, isolated boudins (Fig. 2B) could have formed as segmented thin layers or relics of flattened and dismembered intrafolial fold hinges that developed during transposition of layering (*14*). Many of the discontinuous, single-crystal-thick (millimeter-scale) trains of pyroxenes (Fig. 2, B through D) represent highly stretched boudin tails or occur as veins cross-cutting the foliation. Some thicker pyroxenite layers (as in samples AK 37 and AK 44, Fig. 1C) show pinch-and-swell structure typical of incipient boudinage (*14*), with patchy, but significant, infiltration of quartz in boudin necks (Fig. 2D). Throughout the quartz-pyroxene lithology, we observed only one continuous, thick (~5 cm) pyroxenite band that has not been attenuated into centimeter-scale boudins or strongly infiltrated by quartz (Figs. 1C and 2, A and D; sample AK 38) but is still coaxial with the regional foliation. Collectively, the structural features lead us to conclude that the layering in the quartz-pyroxene rock does not represent a depositional phenomenon, nor does the lithology form part of a conformable depositional package [compare (*1*, *2*)].

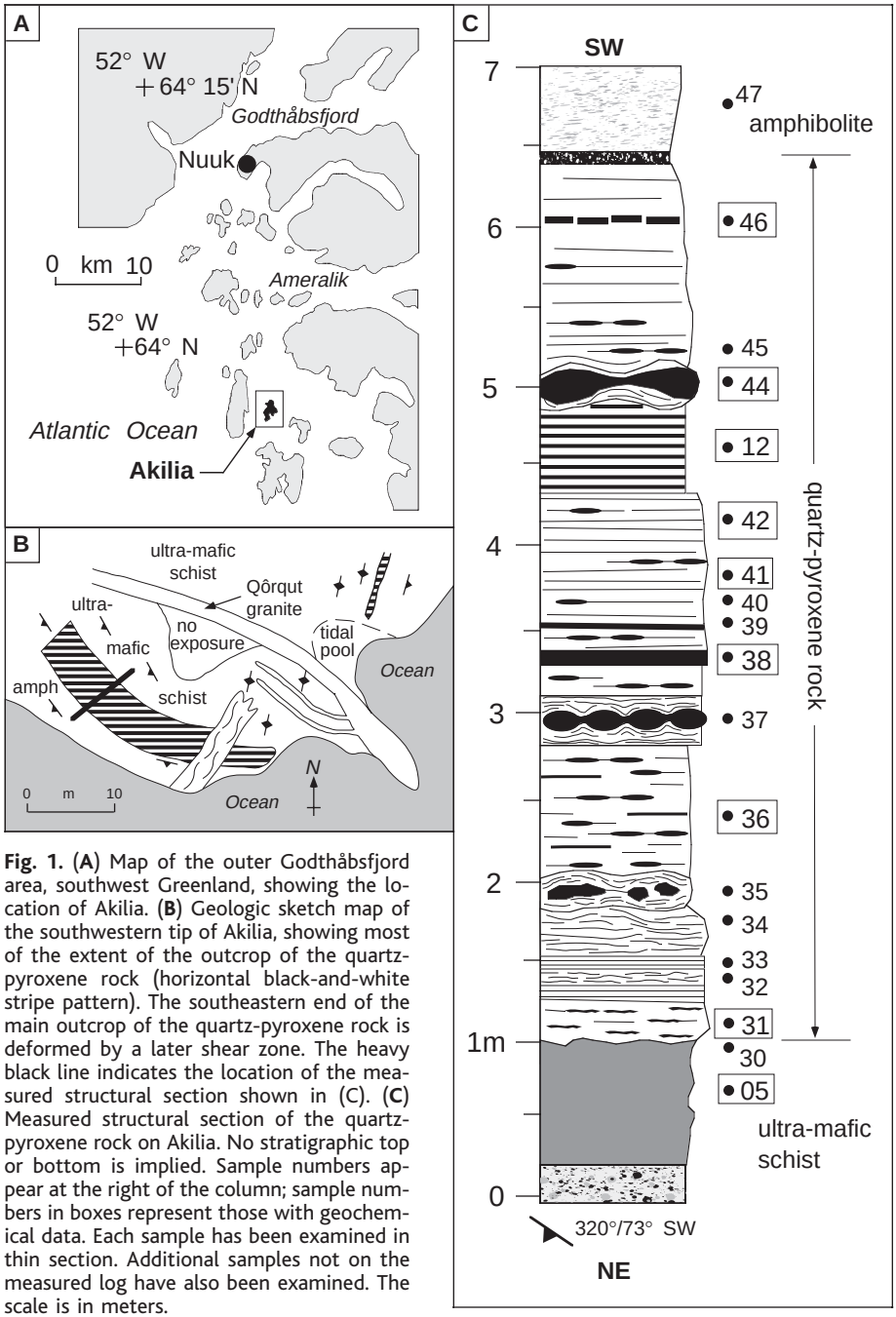

Fig. 1. (**A**) Map of the outer Godthåbsfjord area, southwest Greenland, showing the location of Akilia. (**B**) Geologic sketch map of the southwestern tip of Akilia, showing most of the extent of the outcrop of the quartz-pyroxene rock (horizontal black-and-white stripe pattern). The southeastern end of the main outcrop of the quartz-pyroxene rock is deformed by a later shear zone. The heavy black line indicates the location of the measured structural section shown in (C). (**C**) Measured structural section of the quartz-pyroxene rock on Akilia. No stratigraphic top or bottom is implied. Sample numbers appear at the right of the column; sample numbers in boxes represent those with geochemical data. Each sample has been examined in thin section. Additional samples not on the measured log have also been examined. The scale is in meters.

Rather, all layering represents a tectonic fabric, analogous with millimeter-scale banding commonly exhibited by the adjacent Amîtsoq gneisses.

Modal magnetite is present in two subunits with a combined thickness of about 0.5 m in the ~5-m total thickness of the quartz-pyroxene lithology (samples AK 33 and AK 12, Fig. 1C). In these two subunits, magnetite makes up 5 to 10% of the sample. The remaining subunits contain trace or zero magnetite, their layering consisting typically of millimeter-scale bands of pyroxene with amphibole alternating with centimeter-scale bands of coarse-grained clear quartz (Figs. 1C and 2). Quartz commonly makes up more than 75% of the rock and ranges up to 90%. Minor amounts of pyrite and chalcopyrite are also observed. The presence of magnetite layers at some levels in the quartz-pyroxene rock has been cited as evidence of a sedimentary origin (*2*). However, magnetite occurs in the adjacent ultramafic rocks (as in sample AK 02) and is a potential product of the metamorphic breakdown of siderite (*15*), a metasomatic mineral that was probably present in these rocks, or from serpentinization of olivine-rich precursors (*16*).

To further investigate the origin of these rocks, we present new whole-rock major element, trace element, and rare earth element (REE) data from Akilia (Fig. 3, A through C and table S1) and compare results with the extensive data set for BIFs from Isua, which have been divided into six groups (*17*), and with komatiite-tholeiite compositions from the ~3.5 billion-year-old Barberton greenstone belt (*18*). Even when formed in deep-sea settings, bona fide BIFs have a chemistry that is distinct from that of mafic and ultramafic igneous rocks, because the trace element inventory of seawater, from which BIFs form, is different from that of a mantle source.

The four analyzed ultramafic schists bordering the quartz-pyroxene lithology on Akilia have high Cr [~3500 parts per million (ppm)], high MgO [~21 weight % (wt %)], low SiO_2 (~48 wt %) contents, and a low Th/Sc ratio (0.03) consistent with an ultramafic igneous protolith (*18*) (Fig. 3, B and C). The chemistry of the thin-banded quartz-pyroxene rocks is different, except for the sample from the thick pyroxenite band (AK 38) (Figs. 1C and 2, A and D). The trace element geochemistry of AK 38 is more similar to that of the surrounding ultramafic rocks. It has 2200 ppm Cr, a Th/Sc ratio of 0.01, and a Cr/Th ratio of ~20,000, which are all very different from BIFs in the Isua greenstone belt (Fig. 3B).

REE patterns of samples of quartz-pyroxene rock parallel those of sample AK 38 on a chondrite-normalized plot (Fig. 3A), indicating that all the samples are integrally related. The only major difference is in total abundance, which is much lower in the quartz-pyroxene rocks because of dilution by quartz. Pyroxenite boudins extracted from the unit are also similar to AK 38 in composition and abundance (Fig. 3A). We conclude that although some major element and trace element geochemical comparisons between AK 38 and the remainder of the quartz-pyroxene unit are not easily reconcilable, the REE compositions demonstrate a shared protolith.

All of the quartz-pyroxene rocks on Akilia exhibit concave downward patterns in the light REEs (LREEs) (La through Nd) and a negative slope across the heavy REEs (HREEs) ($Gd_N/Yb_N > 1$), whereas the average Isua BIF pattern is concave upward in the LREEs and has a positive slope across the HREEs ($Gd_N/Yb_N < 1$) (Fig. 3A). Further, on a number of differentiation plots, the quartz-pyroxene rocks (including AK 38 and boudin samples) are closely associated with ultramafic rocks [average komatiite (*19*) and komatiites from Barberton (*18*)] but are distinct from all of the six groups of BIFs from Isua (*17*), from BIFs anywhere else (*20*), or from mafic igneous rocks (*18*, *21*) (Fig. 3C). Exceptions to this occur when elements are strongly partitioned by certain accessory minerals (such as Cr in chromite).

Both modern and ancient uncontaminated BIFs and microbialites are characterized by strong, positive, shale-normalized (sn) (*22*) La anomalies [expressed as (Ce/Ce*)sn (*23*–*25*)]. If the quartz-pyroxene rock on Akilia represents a pure BIF, samples of this rock should show (Ce/Ce*)sn < 1. However, the quartz-pyroxene rocks, including sample AK 38, possess no significant La anomaly (table S1) but rather are similar to Akilia ultramafic rocks. These data and the rest of the trace element geochemistry suggest that a BIF origin for any of the analyzed quartz-pyroxene rock samples is unlikely.

On the basis of our observations and data, we propose that the quartz-pyroxene rocks on Akilia originated as ultramafic intrusions or volcanic rocks, and therefore the carbon isotope signature of contained graphites (*1*) is not indicative of past life. After crystallization, these rocks were compositionally modified during repeated episodes of metasoma-

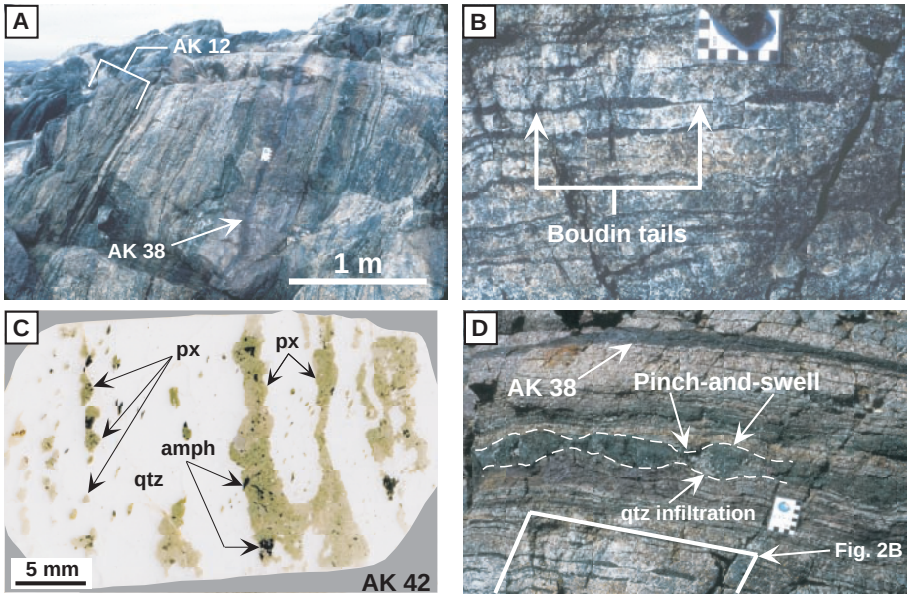

Fig. 2. (**A**) Photograph looking northwest at the main exposure of quartz-pyroxene rock. Note the location of the continuous black band (AK 38) contained in the middle part of the unit. The bracket shows the extent of the outcrop of magnetite-bearing lithology represented by sample AK 12 [probably equivalent to sample G91-26 in (*2*)]. Scale bar, 1 m. Note the abundance of quartz in the overall outcrop. Dark bands are defined by pyroxene (dominant) and amphibole (subordinate). The location of the measured section is shown in Fig. 1C; coordinates are as follows: 63°55.743'N, 51°41.081'W. (**B**) Close-up photograph from the vicinity of sample AK 36, showing millimeter-scale banding in the quartz-pyroxene lithology being generated as tails of pyroxene boudins. Boudinage is a prevalent texture in this lithology, and much of the fine banding is interpreted to have formed this way. Scale is in centimeters. (**C**) Scanned full thin-section photomicrograph of sample AK 42, which is typical of most variants of the quartz-pyroxene rock. Note the discontinuous nature of banding and the invasion of quartz at nearly all scales. Mafic bands on the left side of the image are defined by discontinuous trains of single-crystal–wide pyroxene crystals. Pyroxene is olive green; amphibole is very small dark specks; quartz is white. Magnetite abundance is 0.1% based on 799 points counted. Abbreviations: px, pyroxene; amph, amphibole; qtz, quartz. (**D**) Outcrop photograph showing the location and characteristics of sample AK 38. Note the thick mafic layer below AK 38, showing pinch-and-swell structure (outlined for clarity). The box outlines the area of the photograph in (B). Scale is in centimeters.

tism [including carbonate replacement (*26*, *27*), quartz veining and LREE addition] and metamorphism, whose intensity precludes constraining their timing and number. An ultramafic protolith for the quartz-pyroxene rocks warrants further consideration of the origin of isotopically light graphite inclusions in apatite (*1*). At least two abiotic mechanisms for generating such graphite and magnetite may be identified that are consistent with our interpretations. First, decarbonation of metasomatized ultramafic rock (*26*, *27*) during prograde granulite facies metamorphism at $T > 600$°C (*11*, *15*), accompanied by a Rayleigh distillation process [compare <500°C (*28*)], is theoretically capable of producing magnetite, leaving ^{13}C-depleted graphite and creating a rock devoid of precursor metasomatic carbonate minerals. A second, and geologically more likely, scenario involves a combined process of (i) serpentinization of olivine-bearing ultramafic rocks, in which oxidation of olivine produces both molecular hydrogen from water and magnetite with (ii) metamorphic decarbonation of replaced ultramafic rocks (*26*). This provides a CO_2-rich environment (*29*) needed for abiotic synthesis of hydrocarbons via Fischer-Tropsch type reactions (*16*, *30*, *31*). In this scenario, metasomatically or metamorphically generated magnetite acts as a catalyst, yielding abiogenic hydrocarbons that have δ^{13}C values <–20 per mil, relative to the Pee Dee belemnite standard (*29*). Intense metamorphism postdating this process has resulted in a quartz-pyroxene rock that includes minor, isotopically light graphite. Another possible source for the graphite involves the introduction of a biogenic contaminant [for example, (*32*)] before apatite crystallization, which cannot be entirely dismissed in rocks that have experienced such considerable hydrothermal activity over long periods of time. U-Pb dating of the host apatite (*33*) indicates that they grew (or were reset) at ~1500 Ma, consistent with a metasomatic origin [compare (*34*)], which is corroborated by common apatite in sample AK 44 (a pyroxenite boudin, Fig. 1C).

What evidence can be used to unequivocally define the past existence of life in very ancient rocks? A biological origin for "morphological" fossils from the ~3465 million-year-old Apex chert in western Australia, long thought to represent the oldest physical evidence for life on Earth (*35*), has been recently questioned (*36*), leaving open the possibility that even distinct shapes and organic chemical signatures cannot offer proof. The present paper indirectly questions the veracity of carbon isotope data and indicates that the interpretation of such "chemo- fossils" must be accompanied by a detailed geologic and geochemical assessment of the host rocks. Given these constraints, the best documented evidence for the earliest life on Earth is ^{13}C-depleted graphite particles in deep-sea clastic sedimentary rocks from the Isua greenstone belt at 3700 to 3800 Ma (*37*), which were deposited close to the end of the late heavy asteroid bombardment (*38*), when Earth's surface conditions were more stable and retention of a life-sustaining hydrosphere was favored.

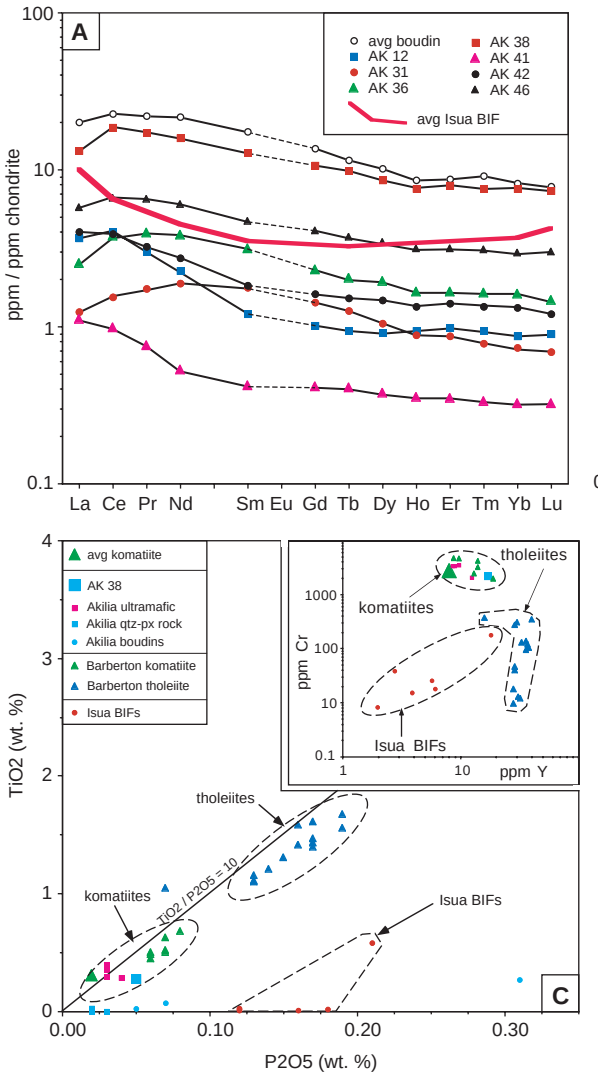

Fig. 3 (**A**) Plot of chondrite-normalized (*39*) REE abundances for the quartz-pyroxene rock. Note the concave-down behavior of the LREEs in the Akilia quartz-pyroxene samples and the concave-up behavior of the LREEs and the entire pattern for average Isua BIF (heavy red line). The scatter of REE abundances in the quartz-pyroxene samples is due to quartz dilution (AK 46 has 71.9 wt % SiO_2; AK 41 has 95.5 wt % SiO_2). The average value of extracted boudins from the quartz-pyroxene rock is similar to AK 38 in composition and abundance of REEs. Analyses for Eu are not plotted because of very inconsistent behavior of Eu. Eu/Eu* (chondrite-normalized) ranges from 0.25 to 1.61, suggesting that metamorphic conditions may have fluctuated near the Eu(II)-Eu(III) valence boundary. (**B**) The plot shows the relationships of the six BIF groups from Isua, average komatiite (*19*), AK 38, and four samples of ultramafic schist from Akilia. None of the six groups of Isua BIF have Cr/Th or Th/Sc ratios near those of AK 38 (a proxy for the entire quartz-pyroxene lithology), which are very similar to those of average komatiite. (**C**) The main plot shows data from Akilia, BIFs from Isua, and tholeiite-komatiite compositions from the Barberton greenstone belt (*18*) for TiO_2 versus P_2O_5. Tholeiites and komatiites plot in consistent positions where $TiO_2/P_2O_5 \leq 10$. AK 38 and Akilia ultramafic samples plot in the komatiite field; all samples of the quartz-pyroxene rock (except for a single boudin) plot near this field. Isua BIFs all lie in an unrelated field. The outlier point in the BIF data represents an aluminous BIF group, which has been interpreted to represent an admixture of BIF and mafic volcaniclastic component and so is not an exclusive BIF composition (*17*). The inset plot shows distinct fields for the different lithologies. Akilia ultramafic samples and AK 38 lie in the komatiite field. Note the distinct position of the Isua BIFs.

References and Notes

1. S. J. Mojzsis *et al.*, *Nature* **384**, 55 (1996).
2. A. P. Nutman, S. J. Mojzsis, C. R. L. Friend, *Geochim. Cosmochim. Acta.* **61**, 2475 (1997).
3. S. J. Mojzsis, T. M. Harrison, *Geol. Soc. Am. Today* **10**, 1 (2000).
4. C. F. Chyba, *Geochim. Cosmochim. Acta.* **57**, 3351 (1993).
5. K. A. Maher, D. J. Stevenson, *Nature* **331**, 612 (1988).
6. A. P. Nutman *et al.*, *Precambrian Res.* **78**, 1 (1996).
7. M. J. Whitehouse, B. S. Kamber, S. Moorbath, *Chem. Geol.* **160**, 201 (1999).
8. B. S. Kamber, S. Moorbath, *Chem. Geol.* **150**, 19 (1998).
9. M. J. Whitehouse, B. S. Kamber, S. Moorbath, *Chem. Geol.* **175**, 201 (2001).
10. V. R. McGregor, B. Mason, *Am. Mineral.* **62**, 887 (1977).
11. W. L. Griffin, V. R. McGregor, A. Nutman, P. N. Taylor, D. Bridgwater, *Earth Planet. Sci. Lett.* **50**, 59 (1980).
12. J. S. Myers, J. L. Crowley, *Precambrian Res.* **103**, 99 (2000).
13. J. S. Myers, *Precambrian Res.* **105**, 129 (2001).
14. B. E. Hobbs, W. D. Means, P. F. Williams, *An Outline of Structural Geology* (Wiley, New York, 1976).
15. E. C. Perry Jr., S. N. Ahmad, *Earth Planet. Sci. Lett.* **36**, 280 (1977).
16. N. G. Holm, J. L. Charlou, *Earth Planet. Sci. Lett.* **191**, 1 (2001).
17. R. F. Dymek, C. Klein, *Precambrian Res.* **19**, 247 (1988).
18. T. W. Vennemann, H. S. Smith, *Geol. Soc. Am. Spec. Pap.* **329**, 133 (1999).
19. K. C. Condie, *Chem. Geol.* **104**, 1 (1993).
20. C. Klein, N. Beukes, in *The Proterozoic Biosphere: A Multidiscipliary Approach*, J. W. Schopf, C. Klein Eds. (Cambridge Univ. Press, Cambridge, 1992), pp. 139–146.
21. The few analyses of mafic and ultramafic rocks from Isua [reported in A. P. Nutman, *Grøn. Geol. Unders. Bull.* **154**, 80 (1986) and (*26*)] are very similar to those of less deformed and metamorphosed equivalents in the Barberton greenstone belt (*18*).
22. Normalization values of Post-Archean Australian Average Shale are from S. M. McLennan, in *Geochemistry and Mineralogy of Rare Earth Elements*, B. R. Lipin, G. A. McKay, Eds. (Mineralogical Society of America, Washington, DC, 1989), vol. 21, chap. 7.
23. Because Pr is not expected to show anomalous behavior, a combined analysis of (Ce/Ce*)sn and (Pr/Pr*)sn provides a measure of La and Ce anomalies, respectively (*24*, *25*).
24. M. Bau, P. Dulski, *Precambrian Res.* **79**, 37 (1996).
25. B. S. Kamber, G. E. Webb, *Geochim. Cosmochim. Acta.* **65**, 2509 (2001).
26. N. M. Rose, M. T. Rosing, D. Bridgwater, *Am. J. Sci.* **296**, 1004 (1996).
27. M. T. Rosing, N. M. Rose, D. Bridgwater, H. S. Thomsen, *Geology* **24**, 43 (1997).
28. J. M. Eiler, S. J. Mojzsis, G. Arrhenius, *Nature* **386**, 665 (1997).
29. P. Szatmari, *Am. Assoc. Petrol. Geol. Bull.* **73**, 989 (1989).
30. J. Horita, M. E. Berndt, *Science* **285**, 1055 (1999).
31. M. S. Lancet, E. Anders, *Science* **170**, 980 (1970).
32. A. Lepland, M. van Zuilen, G. Arrhenius, *Eos* **82**, abstract P22B-0545 (2001).
33. Y. Sano, K. Terada, Y. Takahashi, A. P. Nutman, *Nature* **400**, 127 (1999).
34. S. J. Mojzsis, T. M. Harrison, G. Arrhenius, K. D. McKeegan, M. Grove, *Nature* **400**, 127 (1999).
35. J. W. Schopf, *Science* **260**, 640 (1993).
36. M. D. Brasier *et al.*, *Nature* **416**, 76 (2002).
37. M. T. Rosing, *Science* **283**, 674 (1999).
38. G. Arrhenius, A. Lepland, *Chem. Geol.* **169**, 69 (2000).
39. E. Anders, N. Grevesse, *Geochim. Cosmochim. Acta.* **53**, 197 (1989).

40. We acknowledge research grants from the National Geographic Society and George Washington University to C.M.F. and grants 11595-305 and 11595-306 from the Swedish Research Council (VR) to M.J.W. The Greenland Home Rule Government generously provided permission to conduct studies and collect samples from protected outcrops on Akilia. We also thank S. Moorbath, V. L. Pease, L. L. Sørensen, G. M. Young, B. S. Kamber, M. Rosing, J. M. Hanchar, J. M. Bailey, R. Tracy, J. F. Lewis, and G. Goodfriend for helpful discussions, support, and comments.

Supporting Online Material
www.sciencemag.org/cgi/content/full/296/5572/1448/DC1
table S1

29 January 2002; accepted 8 April 2002

Excavation of a Chimpanzee Stone Tool Site in the African Rainforest

Julio Mercader,[1]* Melissa Panger,[1] Christophe Boesch[2]

Chimpanzees from the Taï forest of Côte d'Ivoire produce unintentional flaked stone assemblages at nut-cracking sites, leaving behind a record of tool use and plant consumption that is recoverable with archaeological methods. About 40 kilograms of nutshell and 4 kilograms of stone were excavated at the Panda 100 site. The data unearthed show that chimpanzees transported stones from outcrops and soils to focal points, where they used them as hammers to process foodstuff. The repeated use of activity areas led to refuse accumulation and site formation. The implications of these data for the interpretation of the earliest hominin archaeological record are explored.

Ape ethoarchaeology uses primatological data to formulate archaeological hypotheses (*1–3*). For example, several authors have studied stone tools used by chimpanzees for nut cracking and have discussed similarities between them and early hominin tools (*1–3*). This paper reports on the nature and content of a naturally buried stone assemblage produced by the nut-cracking activities of chimpanzees (*Pan troglodytes*) in the wild. We describe the behavioral data unearthed at the chimpanzee stone tool site of Panda 100 (hereafter P100) at Taï National Park, Côte d'Ivoire, which was excavated with the same techniques that are applied to the recovery of early archaeological sites and yielded preserved activity areas containing a large amount of plant refuse and 479 stone pieces.

Several West African chimpanzee populations use stone tools to crack open hard-shelled nuts. Nut-cracking technology allows chimpanzees to obtain more than 3000 calories per day (*2*) and has been extensively studied at Taï National Park, Côte d'Ivoire (*2*, *4*). At Taï, chimpanzees are known to crack nuts from *Panda oleosa*, *Coula edulis*, *Parinari excelsa*, *Sacoglottis gabonensis*, and *Detarium senegalense* (*2*). On soft shells (such as those of *Coula*),

[1]Department of Anthropology, George Washington University, 2110 G Street NW, Washington, DC 20052, USA. [2]Max Planck Institute for Evolutionary Anthropology, Inselstrasse 22, 04103, Leipzig, Germany.
*To whom correspondence should be addressed. E-mail: madrid@gwu.edu

Table 1. Size of stone pieces from P100 and selected Early Oldowan assemblages.

Size range (mm)	P100 (%) (granitoid rocks laterite; n = 479)	Omo 123 (%) [quartz (*15*); n = 223]*	Shungura formation, FtJi1 (%) [quartz (*16*); n = 130]	KBS (%) [basalt (*17*); n = 139]†
1–10	49	36	19	16
11–20	30	46	60	27
21–30	7	16	18	19
31–40	4	2	3	14
41–50	4	0.1	0	8
51–60	3	0	0	9
61–70	1	0	0	3
71–80	1	0	0	2
81–90	0.3	0	0	1
91–100	0.3	0	0	0
101–110	0.3	0	0	1

*Numbers only include excavation data. †Flakes = 97.7% of the total assemblage; estimates are based on interpretation of Fig. 1.